

Electrodeposition of Platinum on Nanometer-Sized Carbon Electrodes

Shengli Chen and Anthony Kucernak*

Department of Chemistry, Imperial College London, London SW7 2AZ, U.K.

Received: April 4, 2003

Results for the electrodeposition of platinum on carbon electrodes of nanometer size are presented. It is shown that electrodes with very small electroactive areas simplify the study of the nucleation and growth mechanism involved in electrodeposition. Reducing the electroactive area of the substrate easily controls the number of nucleation sites. With the use of substrates having electroactive radii of a few nanometers, it is possible to form only one single growth center and to allow that center to grow independently. The current transient associated with the growth of such a single nucleus provides both kinetic and mechanistic information about the electrodeposition process. A mathematical formula for the current transient under combined electrokinetic and mass-transport control based on the work of Fletcher [*J. Cryst. Growth* **1983**, 62, 505] and Kruijt et al. [*J. Electroanal. Chem.* **1994**, 371, 13] is used to fit the transients to extract the exchange current density and diffusion coefficient of the reactants. For the Pt on carbon deposition process at low overpotentials, for which the electron-transfer steps control the overall deposition process, single nucleation is observed when the electrode is smaller than about 5 nm in size. It is found that the single nucleation and growth processes can also occur at relatively large electrodes (~100 nm in size) when a high overpotential is applied so that a diffusion-controlled deposition process is established. Such a phenomenon is analyzed in terms of the depletion layer of electroactive species around the growing nucleus, and the effect that this has on the nucleation rate on the surrounding electrode surface.

1. Introduction

Carbon-supported small Pt particles are of great relevance in the catalysis of various electrochemical processes, especially those involved in fuel cells. Electrodeposition has been considered as one approach to produce Pt/carbon electrode assemblies for practical applications or serving as model electrodes for fundamental studies.^{3–5} The Pt/carbon electrode assemblies prepared by electrodeposition on well-defined substrate surfaces generally have reduced structural complexity and are particularly useful for mechanistic investigations. However, electrodeposition is not an ideal way to produce small particles of uniform size because of nonuniform growth of particles and various overlap processes during their formation. The formation of metal particles on macroscopic substrates is generally through a multiple nucleation and growth mechanism. The overlap of individual growing nuclei or the overlap of their diffusion zone occurs very shortly after the nucleation, resulting in the growth of individual centers interfering with one another. In addition, the nuclei are not necessarily born simultaneously because of surface inhomogeneities and the random nature of the formation of stable nuclei. All of these factors prevent the production of small particles with uniform size and geometry. It has been reported that carbon-supported metal particles with very narrow size distribution can be prepared using electrodeposition on highly oriented pyrolytic graphite (HOPG) by stopping the deposition at a very early stage of nuclei growth to avoid the overlap of the diffusion zones of individual growth centers.^{5,6} The electrodes produced in this way have a very low metal loading, which will have a significant impact on the performance of the Pt/carbon assemblies. It has been argued that not only

the particle size but also the separation between adjacent particles affect the performance of Pt/carbon catalytic electrodes.^{7–10} The latter is strongly related to the loading of Pt on the supporting substrate. To increase the Pt loading, longer deposition times have to be used. This will result in overlap and aggregation problems,^{4,5} thereby losing the uniform distribution of particle size and geometry.

The complexities resultant from multiple nucleation and overlap not only limit the practical applications but also complicate the theoretical analysis of electrocrystallization kinetics. To obtain theoretical expressions for the current or potential accompanying the electrodeposition process, some significant approximations have to be introduced to deal with these complexities. For example, two limiting cases are typically assumed when dealing with the nucleation rate, that is, instantaneous nucleation and progressive nucleation. The real deposition processes are rather more complex than such limiting cases. The birth of new nuclei is a random process, and the initiation time of new nuclei has a wide distribution.¹¹ In addition, the problems related to the overlap process have not been fully understood and solved, although Avrami's approximation is generally used.¹²

Most of these theoretical and practical complexities involved in electrodeposition would disappear under the situation of single nucleation and growth. The theoretical analysis of the growth of a single nucleus is straightforward and no assumptions are needed to deal with the nucleation rate or the overlap problems. There are no size and geometrical distribution problems if only one particle exists on the substrate surface.

Two approaches may be taken to force only one particle to exist on the surface. The first is to limit the nucleation-site density on the surface, and the second is to reduce the area of the surface. In the first instance, control may be influenced by

* To whom correspondence should be addressed. E-mail: a.kucernak@ic.ac.uk. Phone: +44 20 75945831. Fax: +44 20 75945804.

the choice of system and substrate and by surface pretreatment—although it must be admitted that control of the density of nucleation sites using this approach is poorly understood. Furthermore, background electrochemical processes occurring on the substrate may mask the currents due to electrochemical nucleation and growth during the initial stages. Thus, the most efficient strategy to control the extent of nucleation is to reduce the electroactive area of the substrate electrodes. With electrodes of micrometer dimensions, single nucleation and growth processes were observed in several deposition processes, such as the deposition of PbO_2 , Hg, and Ag on carbon and platinum substrates.^{13–15} Because the electrode area is still very large compared to the dimension of a stable nucleus, this approach only really works because of the poor nucleation kinetics of the systems used. Recent progress in making nanometer electrodes may open up new opportunities to study the single nucleation and growth process in a much larger number of systems, because it is now possible to produce electrodes with over 6 orders of magnitude decrease in surface area compared to the previous work on microelectrodes. Recently, we have shown that carbon ultramicroelectrodes with extremely small electroactive areas can be fabricated by employing electrochemical etching of a carbon fiber followed by electrophoretic deposition of paint onto the etched fiber.^{16,17} A new approach has been developed, the so-called “inverted deposition” technique, which makes it possible to completely insulate the whole body of the carbon fiber except for the very tip of that fiber, leaving an electrochemical active area with effective radii from several hundred nanometers down to nanometer dimensions. It would be of great significance to use these small carbon electrodes as the substrate for metal deposition. For the smallest electrodes, the resulting electrodes are of the same size as the incipient stable nucleus of a metal cluster, therefore allowing only one stable nucleus to form during the deposition process. Even if multiple nucleation does occur, the number of nuclei formed would be very small and the overlap finished in a very short time to produce a single growth center. The kinetics of electrocrystallization can then be extracted in a straightforward manner from the current–time transient corresponding to the growth of a single particle.

This approach also provides a promising way to prepare very small single Pt particles supported on carbon substrates. By controlling the deposition charge, particles of different size can be prepared. The Pt/carbon electrode assemblies produced thus would be ideal model electrodes for electrocatalytic studies, with such features as high mass-transport coefficient, a single sized distribution, and a well-defined geometry.

In this paper, we present results on the electrodeposition of Pt on nanometer-sized carbon microelectrodes. It is shown that the sizes of the substrate electrodes, as well as the overpotential for the electrodeposition process, are critical parameters in determining the nucleation and growth mechanism of the Pt electrodeposits.

2. Experimental Section

A detailed description for the preparation of nanometer-sized carbon electrodes can be found in refs 16–17. Briefly, these electrodes were made using carbon fibers (PANEX33 CF, 95% carbon, obtained from Zoltek Corporation, MO) as starting material. The carbon fibers were electrochemically etched in 0.05 mol dm^{-3} NaOH solution to form a tapered sharp tip of nanometer dimensions. Such tips were then insulated by deposition of a cathodically deposited electrophoretic paint (Clearclad HSR, LVH Coating Ltd, U.K.). The insulation

process involves two steps, the first being electrophoretic deposition of paint onto the carbon fiber surface and the second step being a curing step at high temperatures to fuse the polymeric insulating film. Some shrinkage of the deposited film occurs during the heating process, and Laplace pressure differences prevent wetting of the tip. To insulate the whole body of the fiber, while still allowing the spontaneous emergence of the very end of the tip, we use the “inverted deposition” process. In this approach, the fiber tip is inverted within the paint solution and translated so that the tip pushes through the surface and draws a meniscus with it. Such an arrangement leads to virtually no deposition at the very end of the tip and an increase in deposition density as one moves away from the tip. The subsequent heat cure process will expose the very end of the tip but, because of the higher density of polymer deposition on the shaft of the electrode, lead to a pinhole-free coating on the main fiber. Scanning electron microscopy (SEM) images showed that the etched tips have a tapered sharp end. The tip radii are below 50 nm. SEM images of the insulated tips with such tiny electroactive areas show no clear interface between the polymer insulation and the exposed carbon fiber tip surface. What can be seen from the SEM images of the insulated tips is a smooth, defect-free insulation layer. Moreover, voltammetric measurements using reversible or quasi-reversible redox couples clearly show that only the tip end is exposed and that the effective electroactive radii of these electrodes range from several nanometers to several hundreds of nanometers, as indicated by the steady-state limiting currents.¹⁷ In this study, the electroactive radii of the substrate carbon electrodes were determined from the steady-state limiting current obtained in $0.010 \text{ mol dm}^{-3}$ $\text{K}_3\text{Fe}(\text{CN})_6$ (BDH AnalaR) + 0.5 mol dm^{-3} KCl (BDH Analar). Such determinations are based on the assumptions that the exposed portion of the insulated fiber tip possesses a hemispherical shape and that the transport of electroactive species toward the electrode is purely through diffusion. Thus, the effective electroactive radius (r_{eff}) has a linear relationship with the measured limiting current (i_d):

$$i_d = HnFDc_{\infty}r_{\text{eff}} \quad (1)$$

where H is a shape factor and equals 2π for hemispherical electrodes (4π for spherical electrodes) and D and c_{∞} are, respectively, the diffusion coefficient and the concentration of electroactive species in the electrolyte. In general, the parameter H is defined as

$$H = 2(2\pi - \theta) \quad (2)$$

where θ is the radial angle subtended by the substrate: $\theta < \pi$ corresponds to a conical substrate; $\theta = \pi$ corresponds to a planar substrate; $\theta > \pi$ corresponds to a conical cavity. This angle results from a consideration of the axisymmetric nature of eq 1. For the particles that we study, θ varies between π and $\pi/2$, Figure 2b.

Electrodeposition of Pt was performed in 0.1 mol dm^{-3} H_2SO_4 (Merck, Aristar) containing $0.001 \text{ mol dm}^{-3}$ H_2PtCl_6 (Alfa). Pure argon gas was bubbled into the electrodeposition solution for 15 min to remove any oxygen prior to each deposition experiment. During the deposition, an argon atmosphere was maintained above the solution. A potential of 0.8 V vs the saturated calomel electrode (SCE) was applied when the carbon substrate electrodes were immersed to prevent spontaneous deposition of Pt. The potential was then stepped from this value to the deposition potential, and the current transient was recorded. All potentials in this paper are quoted against the SCE unless stated.

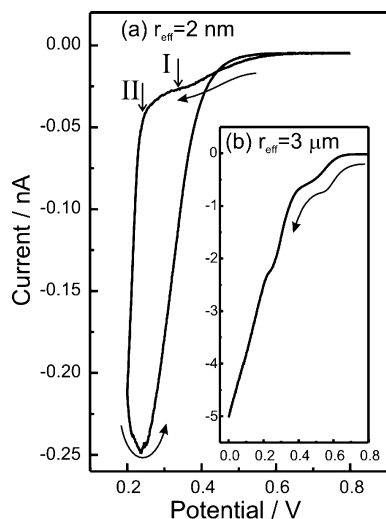


Figure 1. The potentiodynamic I/E profiles obtained in solution of $0.1 \text{ mol dm}^{-3} \text{ H}_2\text{SO}_4 + 0.001 \text{ mol dm}^{-3} \text{ H}_2\text{PtCl}_6$ at carbon fiber microelectrodes having effective radii of (a) 2 nm and (b) $3 \mu\text{m}$ at a scan rate of 0.001 V s^{-1} .

An AutoLab PGSTAT20 potentiostat with an ECD module (Eco Chemie BV, Netherlands) was used in all electrochemical measurements. A two-electrode configuration with a calomel reference electrode as auxiliary separated from the working electrode through a Luggin capillary was employed in those experiments determining the electroactive radius of electrodes and during the electrodeposition of Pt. All solutions were prepared with Milli-Q water, and all experiments were conducted at room temperature.

3. Results and Discussion

3.1. Potentiodynamic Current–Potential Curve Associated with Pt Deposition. In Figure 1, we show potentiodynamic scans of the carbon-substrate microelectrodes in the Pt plating solution to provide some qualitative information of the Pt deposition process. Figure 1a shows a typical cyclic voltammogram (CV) obtained on a nanometer-sized carbon electrode in a solution of $0.1 \text{ mol dm}^{-3} \text{ H}_2\text{SO}_4$ containing $0.001 \text{ mol dm}^{-3} \text{ H}_2\text{PtCl}_6$. A slow potential scan rate (0.001 V s^{-1}) is used so that the quasi-steady-state current–potential profile could be obtained. As shown in the negative going branch, the reduction current starts to develop at about 0.6 V and establishes a poorly defined current plateau extending to about 0.23 V. As the potential is scanned more negative of this point, there is a very steep increase in current.

Typically, during cyclic voltammetry at microelectrodes, a steady-state current plateau is observed due to mass-transport control. In contrast, the results in Figure 1a show that once the potential has been decreased below 0.23 V a hysteresis in the current response as the current reverses direction is seen. Once the scan direction changes to the positive-going branch, the current keeps growing and ends up being much larger than the negative-going branch. Such behavior in cyclic voltammograms is typically observed during the electrochemical formation and growth of a new phase following a nucleation event. This implies that the steeply decreasing reduction current corresponds to the deposition of Pt.

On carbon fiber bundle electrodes, N. Georgolios et al. observed three reduction waves during the reduction of H_2PtCl_6 in the same solution.¹⁸ Similar results were obtained on both HOPG,¹⁹ and glassy carbon²⁰ electrodes. We find that such results occur on a carbon microelectrode that is over 10^3 larger

in radius than that used in Figure 1a. For this electrode, Figure 1b, two clearly separated reduction waves can be observed before the main deposition process. In comparison, in Figure 1a, only one reduction wave is observed before the main deposition peak. Such a single reduction wave before the main deposition process has also been seen during the electrodeposition onto a gold microelectrode from a hexagonal lyotropic liquid crystalline phase of a nanostructured mesoporous platinum film.²¹ We suggest that when the substrate electrode is very small the first reduction wave becomes very irreversible and tends to overlap the second one. Another difference of the CV in Figure 1a from those obtained on macroscopic electrodes is that the current corresponding to the main deposition peak is significantly larger than the current shoulder. If the potential is swept to 0 V, as it is in Figure 1b, the current shoulder is almost unseen in the CV because the current corresponding to the main deposition process is so large. This reveals that the nucleation and growth mechanism is manifested more clearly in the CV on nanometer-sized electrodes.

The reaction associated with the first reduction waves has previously been shown to be a diffusion-controlled process and attributed to the reduction of Pt(IV) to Pt(II) species.¹⁸ The disproportionation of Pt(II) species into Pt(IV) and Pt(0) may also be involved during this reaction.^{19,20} We found that when the potential is stepped to a value in the first reduction wave (i.e., Figure 1a at point I), the current transient shows an initial spike that rapidly decays to a steady-state current, corresponding to the typical diffusion-controlled transient behavior of a microelectrode. Voltammetry on this electrode after the deposition process revealed no indication of Pt voltammetric features such as hydrogen adsorption/desorption, and no activity was seen for oxygen reduction indicating that no Pt had been deposited. In comparison, when the potential was stepped to values located in the second wave (Figure 1a, II), the current transients showed a response typical of a nucleation and growth mechanism, and Pt was detected on the resultant composite electrode.

Displayed in Figure 2 are SEM images of two Pt particles produced on carbon ultramicroelectrodes. In both cases, the potentiostatic transient during the deposition of the particles indicated that a single nucleation–growth event occurred. It can be seen that a spherical, well-formed particle is produced. Figure 3 shows the voltammogram of one such particle in $0.5 \text{ mol dm}^{-3} \text{ H}_2\text{SO}_4$. The electrochemical features of the voltammogram agree well with those expected for platinum except for a slight increase in the separation of the anodic and cathodic branches due to charging of the capacitance of the leads used. The surface area calculated from the hydrogen adsorption region agrees well with the diameter of the particle measured by SEM; in this case, the particle has a radius of 150 nm. In this paper, we will focus on Pt deposition that follows the nucleation and growth mechanism and that leads to the formation of Pt particles of the form shown in Figure 2.

3.2. Current Transients Accompanying Platinum Deposition with a Nucleation and Growth Mechanism—Single Nuclei. The form of the current transients associated with the nucleation and growth mechanism is that of a rising current, which occurs because after the initial potential step a new nucleus is formed and as this nucleus grows there is an increase in its active area. The current–time relationship accompanying the growth of a single nucleus depends on the rate-determining process of the deposition reaction, which is either transport of an active species toward the crystallite nucleus or the electrochemical crystallization process or a combination of both. For

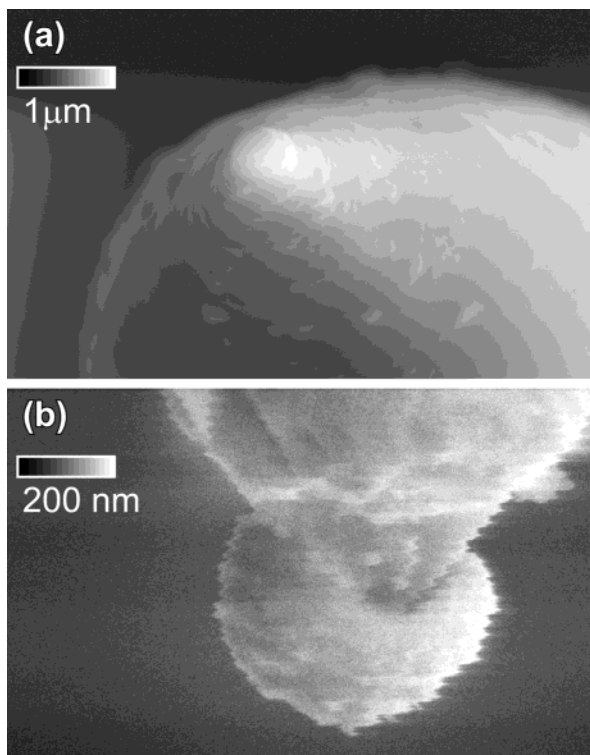


Figure 2. SEM images of two carbon ultramicroelectrode-supported Pt particles. The diameters of the particles are about (a) 300 and (b) 550 nm.

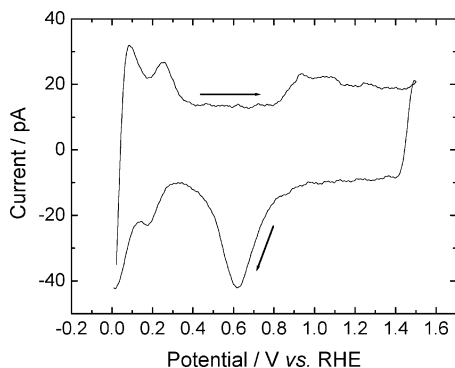


Figure 3. Cyclic voltammogram in 0.5 mol dm⁻³ H₂SO₄ of a carbon ultramicroelectrode-supported Pt particle. The Pt particle has a radius of 150 nm; scan rate was 1.0 V s⁻¹.

three-dimension growth of a single hemispherical nucleus, the radius of the growing particle under pure electrocrystallization control may be expected to increase linearly with time:

$$r(t) = V_M K t \quad (3)$$

where V_M (cm³·mol⁻¹) is the molar volume of the deposited material and K (mol·cm⁻²·s⁻¹) is the rate of the electrocrystallization process, representing the amount of deposition on unit area within unit time interval. We may then use Faraday's law, the relation between the growth current and the cluster radius irrespective of the growth mechanism, that is,¹³

$$i(t) = (FHn/V_M)r^2(dr/dt) \quad (4)$$

to determine the current from eq 3

$$i(t) = FHK^3 n V_M^2 t^2 \quad (5)$$

where H was the geometric factor as previously defined and n is the total numbers of electron involved in the overall process of electrocrystallization. For the case where diffusion controls the growth process, the current corresponding to the growth of a single nucleus has been derived by incorporating Faraday's law into the expression for the steady-state diffusion current toward the growing nucleus,²²

$$i(t) = 1/2 FHn(2Dc_\infty)^{3/2} V_M^{1/2} t^{1/2} \quad (6)$$

Regardless of the process limiting the growth of the single nucleus, it is obvious that the current will continuously increase with deposition time. In reality, it is quite likely that we may have a nucleus that starts growing under electrocrystallization control but for which the growth mechanism switches to diffusion control once that particle reaches a suitable size.

Thus a more complete analysis would entail considering each of these different processes. Furthermore, an added subtlety is that the overpotential driving the electrocrystallization process needs to be corrected for the concentration overpotential and any ohmic losses about the growing nucleus. Kruijt et al.² (and before that Fletcher¹) have provided such an analysis. We refer the reader to these papers for a discussion of the approach to these derivations.

The overpotential driving the deposition process, η , is the difference between the applied potential, ΔE , and the sum of the concentration overpotential, η_C , and ohmic overpotentials, η_Ω .

$$\eta = \Delta E - \eta_C - \eta_\Omega \quad (7)$$

In our analysis, we assume that the presence of a supporting electrolyte, combined with the very small currents measured, makes the ohmic overpotential negligible. Under these conditions, the instantaneous deposition current at a particle of radius r is

$$i(t) = HJ_0 r^2 \left\{ \frac{c_s}{c_\infty} \exp\left(\frac{\alpha n F \Delta E}{RT}\right) - \exp\left(\frac{-(1-\alpha)n F \Delta E}{RT}\right) \right\} \quad (8)$$

where c_s is the concentration of the electroactive species at the surface of the growing particle. The current is also related to the diffusional flux of the reacting species to the surface of the growing particle

$$i(t) = DFHnr^2 \left(\frac{dc}{dx} \right) = c_\infty DFHnr \left(1 - \frac{c_s}{c_\infty} \right) \quad (9)$$

The last term in eq 9 is derived in ref 2 as

$$\left(\frac{c_s}{c_\infty} \right) = 1 - \frac{r^2}{c_\infty 2DV_M t} \quad (10)$$

Eliminating the current between eqs 8 and 9 and substituting the value for c_s/c_∞ from eq 10, we obtain an expression for the radius of the growing particle as a function of time

$$r(t) = \frac{\sqrt{A^2 + 8ABV_M t} - A}{2C}$$

$$A = c_\infty DFn$$

$$B = \frac{j_0^2}{Fn} \left(\exp\left(\frac{2\alpha nF\Delta E}{RT}\right) - \exp\left(\frac{(2\alpha - 1)nF\Delta E}{RT}\right) \right)$$

$$C = j_0 \exp\left(\frac{\alpha nF\Delta E}{RT}\right) \quad (11)$$

This equation is a more general form of the equations given by Kruijt et al.² and Fletcher.¹ Substituting this equation into Faraday's equation, eq 4, we obtain a rather complicated equation for the current as a function of time for the growth of a particle under combined electrokinetic and mass-transport control

$$i(t) = \frac{ABFn(\sqrt{A^2 + 8ABV_M t} - A)^2}{2C^3 \sqrt{A^2 + 8ABV_M t}} \quad (12)$$

This equation correctly predicts the required limiting responses: an approximately quadratic increase of current with time under conditions where electrokinetic control would be expected to predominate (i.e., high diffusion coefficients/reactant concentration or low exchange current density/overpotential or both) and a $t^{1/2}$ dependence when diffusion control would be expected.

The point at which the growth mechanism switches over from electrokinetic control to diffusion control may be determined from the inflection point of the current–time curve, that is, by determining the second derivative and solving for t

$$t_{\text{changeover}} = \frac{A}{4BV_M} \quad (13)$$

where A and B are defined above. For Pt deposition on the nanometer-sized carbon electrodes in this study, current transients corresponding to a nucleation and growth mechanism are mostly observed when the deposition potential is below 0.3 V. Either single nucleation or multiple nucleation processes may occur depending on the size of the substrate electrode and the deposition potential. When the deposition potential is greater than 0.2 V, current transients generally show characteristics of an electrocrystallization-controlled nucleation and growth mechanism, that is, a clearly defined initial period over which the current rises in an approximately quadratic fashion. The period over which the current shows this quadratic behavior with time becomes shorter as the applied potential becomes more negative than 0.2 V. When the potential is lower than 0 V, a well-defined region at short times is observed during which the current is linear with the square root of time. This indicates that diffusion governs the deposition process at sufficiently high overpotentials. Current transients corresponding to these two different cases are shown in the following two subsections.

3.2.1. Deposition and Growth of Pt on Small Electrodes at Low Overpotentials—Electrocrystallization Control. In Figure 4, we plot examples of transients during the electrodeposition of Pt under relatively low overpotentials at which we might expect the growth to be predominantly under electrocrystallization control. At short time, there is a quick decay in current followed by a plateau, a variable induction period, and subsequently a growth in current attributed to the nucleation and growth of a Pt particle.

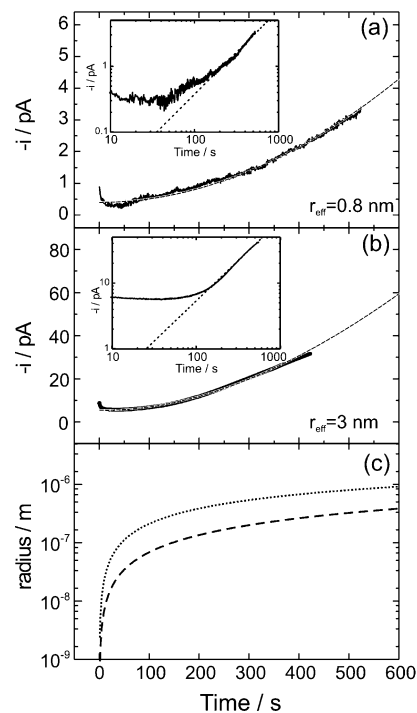


Figure 4. Current–time curves after potential steps from 0.8 to (a) 0.3 and (b) 0.27 V obtained at electrodes of (a) 0.8 and (b) 3 nm in 0.1 mol dm⁻³ H₂SO₄ + 0.001 mol dm⁻³ H₂PtCl₆: (—) current transient; (---) fit to eq 12. The insets show log–log plots of the transients along with linear fits to the later time response. Panel c shows the calculated radii as a function of time from the fitted curves in (—) panel a and (···) panel b. Parameters used for the simulations were $\alpha n = 1$, $c_\infty = 1.0 \times 10^{-6}$ mol cm⁻³, $T = 298$ K, $V_M = 9.1$ cm³ mol⁻¹, $H = 2\pi$, and $D = 1.2 \times 10^{-5}$ cm² s⁻¹. Background currents were (a) 0.4 and (b) 5.5 pA.

In both cases, the current is offset from the baseline. The electrodeposition of platinum from PtCl₆²⁻ solutions may involve the following processes:²³



For those cases in which the current transient did not show an obvious nucleation and growth process, the resultant electrode showed no indication of any platinum deposition, that is, no obvious hydrogen underpotential deposition (UPD) peaks can be found and no obvious activity for oxygen reduction is seen. This indicates that the reactions involved in the initial current transient and the following induction period contribute very little to the formation of a stable Pt deposit. A detailed analysis of the possible reactions occurring during the current decay sections of the chronoamperograms may be found in ref 19. Under the conditions of these experiments and at relatively short time, we expect that the major reaction occurring on the carbon electrode is the homogeneous reduction of PtCl₆²⁻, reaction I. It is only at longer times, once a Pt nucleus is formed and once the size of that nucleus approaches that of the underlying carbon electrode, that the net current becomes dominated by the growth of the Pt particle. Separate experiments performed in our laboratory suggest that the homogeneous reduction of the hexachloroplatinate(IV) anion as embodied by reaction I does not occur on Pt to a significant extent and that on Pt the vast

majority of the current is due to the further deposition of Pt metal. We now mainly focus on the nucleation and growth process.

Log–log plots of the current transients are portrayed in the insets in Figure 4a,b and provide information about the mechanism of growth of the particles. At long times, the time exponents have values of 1.28 ± 0.01 and 1.224 ± 0.001 for the insets within Figure 4, panels a and b, respectively. These exponents are less than the value of 2 expected for a reaction under pure electrocrystallization control. This suggests that although the growth of platinum on these electrodes is predominantly under electrocrystallization control, there is some component of diffusional limitation present. Plotted in the main diagrams for Figure 4 are the fits to eq 12 for the entirety of the two transients assuming common values of all of the parameters apart, of course, from the deposition potentials. The only freely adjustable parameter in these fits is the exchange current density, j_0 . We presume a value of 2π for H , and assume that $\alpha n = 1$, the only value that gives reasonable fits to both transients. To account for the homogeneous reduction of PtCl_6^{2-} following reaction I, we correct for the background current. We utilize a value for the diffusion coefficient of $1.2 \times 10^{-5} \text{ cm}^2 \text{ s}^{-1}$ determined below. We assume that the reaction follows scheme III and calculate the applied potential (ΔE) from the standard potential for this reaction. We obtain a value for j_0 of $(8 \pm 1) \times 10^{-6} \text{ A cm}^{-2}$.

At short time, the currents are larger than those predicted by the curve determined from eq 12. This deviation is probably the result of complexities in the reduction of PtCl_6^{2-} as previously mentioned.

Utilizing the above parameters, we calculate the radii of the Pt nuclei in Figure 4a,b assuming 100% deposition efficiency and plot these as a function of time in Figure 4c. The ultimate nuclei are expected to have radii of 400 nm and $1 \mu\text{m}$, respectively, close to what is determined experimentally. As can also be seen from Figure 4c, the nuclei initially grow very quickly in size and within a few seconds are larger than the underlying electrode. This precludes the possibility of multiple nucleation and growth having any effect on the transients in Figure 4.

3.2.2. The Effect of Electrode Size on Pt Electrodeposition at Low Overpotentials. Under conditions of low overpotential, the transients observed become quite different once the size of the electrodes become larger than those in Figure 4. Displayed in Figure 5a are $\log(i) - \log(t)$ plots obtained during the electrodeposition process at electrodes with radii ranging from approximately 1 to 150 nm. There always is uniform or slightly decreasing current before the rising current due to the deposition of the platinum on the electrode. An initial drop in current has often been commented upon during the electrodeposition of Pt on carbon substrates and has been ascribed to the formation of a Pt monolayer or the random deposition of small Pt clusters,^{4,24} although, at least for our experiments, this seems unlikely because the charge associated with the initial transients are too large.

We found that this falling section becomes more pronounced when larger substrate electrodes or lower overpotentials were used. At larger electrodes or when the deposition potential is higher than 0.25 V, an induction time is observed before the increase in current due to nucleation and growth of the Pt particle. The magnitude of the limiting current during the induction period is linearly dependent on the radius of the electrode as shown in Figure 5b. We attribute this limiting

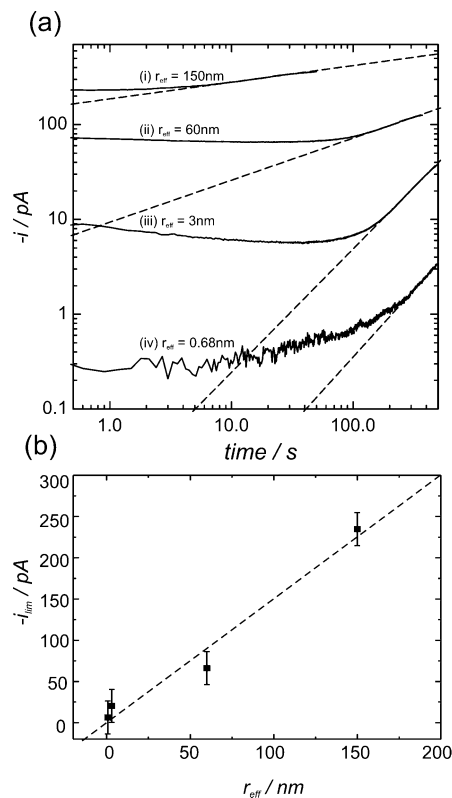


Figure 5. Current–time curves (a) after potential steps from 0.8 to (i) 0.28, (ii) 0.3, (iii) 0.27, and (iv) 0.3 V. The effective radii of the underlying carbon electrodes are displayed on the graph. Panel b shows the initial limiting current as a function of effective electrode radius. Solution composition was $0.1 \text{ mol dm}^{-3} \text{ H}_2\text{SO}_4 + 0.001 \text{ mol dm}^{-3} \text{ H}_2\text{PtCl}_6$.

current to the two-electron homogeneous reduction of Pt(IV) to Pt(II) on the carbon electrode, reaction I.

From the slope of the best fit line in Figure 5b and using eq 1, we calculate a diffusion coefficient for the hexachloroplatinate(IV) anion of $(1.2 \pm 0.1) \times 10^{-5} \text{ cm}^2 \text{ s}^{-1}$. The average value for the diffusion coefficient that we obtain is about three times higher than that obtained by K. Shimazu et al.²⁰ and by F. Gloaguen et al.;⁴ however, it is about 4–5 times smaller than those obtained by A. Kelaidopoulou et al.²⁵ K. Shimazu et al.²⁰ conducted measurements on activated glassy-carbon electrodes upon which falling current transients were obtained when the potential was stepped to very low values located at the third reduction wave on carbon macroelectrodes. A diffusion coefficient of $4.5 \times 10^{-6} \text{ cm}^2 \text{ s}^{-1}$ for PtCl_6^{2-} was estimated from the slope of the Cottrell plots. With the use of HOPG as substrate electrodes, nucleation and 3-D growth current transients were observed on the reduction of PtCl_6^{2-} and a diffusion coefficient values of $3.4 \times 10^{-6} \text{ cm}^2 \text{ s}^{-1}$ was calculated by F. Gloaguen et al.⁴ The measurements by A. Kelaidopoulou et al. were performed on well-polished tungsten electrodes and a diffusion coefficient value of $5.47 \times 10^{-5} \text{ cm}^2 \text{ s}^{-1}$ was extracted from the current transients of nucleation and growth process.²⁵ Although the measurements conducted in this study may have some uncertainties, the estimated values of diffusion coefficient are still reasonable compared to the range of values reported in the literature.

Two other aspects of these transients are obvious. The first is that as the radius of the underlying electrode decreases, the induction time increases; the second is that the slope of the log–log plots changes with the radius of the underlying electrode.

The decreased induction time with electrode radius is undoubtedly due to the random nature of the initial deposition of the Pt particle. The induction period can last significant lengths of time and increases as the radius of the underlying carbon electrode decreases, indicating that the probability of a nucleation event is small and proportional to the area of the electrode. As the radius of the underlying carbon electrode is increased, the surface area of that electrode will increase quadratically. Assuming that the probability of nucleation is uniform across the entire surface of the electrode, the number of active nucleation sites at a given time after the transient begins should also increase at up to a quadratic rate (the exact law will depend on the degree of collision or amalgamation of the growing nuclei and the extent to which the growing nuclei produce an exclusion zone around them due to depletion of reactants). Interestingly, we find that when the effective electroactive radius of the substrate electrode is less than 5 nm the current transient for nucleation and growth can be obtained at potentials even more positive than 0.3 V. Thus an important benefit of using nanometer-sized electrodes is that the current due to the growth of the Pt nuclei quickly outstrips the current due to the homogeneous reduction reaction. This ensures that the deposition process may be studied when the deposited nucleus is still very small. In comparison, at electrodes approaching micrometer sizes, the current transient due to the electrocrystallization process only becomes observable when the deposited platinum particles are of a significant size, that is, relatively late in the growth process.

Typically, we only reproducibly observed transients with time exponents as high as those of Figure 5, curves iii and iv, when the substrate electrode is smaller than 5 nm, as has been shown previously for Figure 4. As the size of the underlying electrode is increased, the exponent decreases ending up close to $1/2$ when the underlying electrode is 60 nm in radius and about 0.2 when the electrode size is 150 nm. Utilizing eq 13 and the parameters for Pt deposition determined above, we would expect the growth of a single particle to switch from predominantly electrokinetic to predominantly diffusion control after about 40 000 s. Thus, it seems probable that the low-time exponents seen for Pt deposition on the larger diameter electrodes are not due to a switchover to a different growth mechanism, rather they are due to multiple nucleation of Pt sites on the electrode. This is further confirmed by the inability to utilize eq 12 to fit the transients on large electrodes, Figure 5, curves i and ii, using the parameters determined during the fitting of transients in Figure 4. In comparison, good fits are obtained to the transients on the smallest electrodes, Figure 5, curves iii and iv.

3.2.3. Single Nucleus Growth under Large Overpotential—Diffusion Control. Figure 6a,b shows two typical current transients accompanying Pt deposition on carbon nanometer electrodes (110 nm and 1 nm, respectively) at potentials more negative than 0 V. Similar to the current transients shown above, a falling current occurs at the beginning of the transients followed by a period over which the current maintains a very low value. This so-called “induction period” varies between experiments. Typically, it is in the range of 1–20 s. Generally, this period is increased at smaller electrodes and at more positive deposition potentials.

A rapidly rising current follows this plateau. Such current transients can be generally observed on carbon nanoelectrodes having effective electroactive radii up to several hundred nanometers. The dotted lines show the fit to these transients utilizing eq 12 and the previously determined parameters. The diffusion coefficient was used as fitting parameter. The diffusion

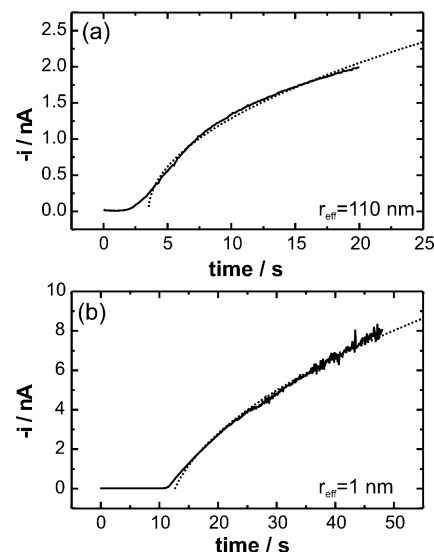


Figure 6. Current transient in 0.1 mol dm⁻³ H₂SO₄ + 0.001 mol dm⁻³ H₂PtCl₆ for (a) 110 and (b) 1 nm carbon microelectrodes after a potential step from 0.8 to -0.1 V: (—) current transient; (···) fit to eq 12. Parameters used for the simulations were $\alpha n = 1$, $c_\infty = 1.0 \times 10^{-6}$ mol cm⁻³, $T = 298$ K, $V_M = 9.1$ cm³ mol⁻¹, $H = 2\pi$, and $j_0 = 8 \times 10^{-6}$ A cm⁻².

coefficient required to produce these fits is $(2 \pm 1) \times 10^{-5}$ cm² s⁻¹, in good agreement with the value previously determined. As we shall show below, this transient is characteristic of a single nucleation and growth process under predominantly diffusion control. Under such high overpotentials, the multiple nucleation and growth process is seldom observed on these small carbon electrodes during the Pt deposition process.

The formation of new nuclei is a result of aggregation of small atom clusters due to surface diffusion along the electrode surface.⁴ The small clusters may also dissolve into the solution. A stable growing center can only be formed when a cluster contains enough atoms and exceeds a critical size. Once such a stable nucleus is formed, spontaneous growth can then easily proceed. Thus, the formation process of a new stable nucleus is actually a competition process between the aggregation and dissolution of atom clusters. Sluyters et al. have developed a model to better understand this nucleation process.²⁶ By assuming certain probability functions for the growth, decline, or stasis of clusters as a function of the cluster size, they find that transients with induction periods similar to those seen in experimental transients may be produced in computer simulations.²⁷ When the electroactive area of the underlying substrate is reduced, the production and enlargement of the clusters become easier because the deposition is focused on a smaller area. In addition, the probability of aggregation of the small clusters would greatly increase with decreasing substrate area.

As well as increasing the probability of nucleation, reduction of the substrate electrode area can also control the number of nucleation events. A stable nucleus may contain several to several tens of atoms depending on the nature of the deposition species and the substrate. We may assume that the size of the stable nucleus for Pt deposition is around 1 nm diameter, corresponding to about 30–40 atoms.⁴ If the substrate has an electroactive area significantly larger than this value, multiple nuclei may be formed, either instantaneously or progressively. It may be expected that only when the electrode size is comparable to the dimension of one stable nucleus will the formation of single growth centers become possible. However, this is not so once a growing nucleus is formed; it will tend to

form a depletion layer around itself in very short time, which has led to the concept of “nucleation exclusion zones” around the growing nucleus.^{28,29} This concept has been considered in most models of progressive nucleation, although typically it is assumed that the nucleation rate is zero in the part of the electrode covered by the concentration and overpotential zones surrounding nucleated particles and maintains some initial value elsewhere. In reality, such a sharp cutoff will not exist, and Milchev et al. have derived an equation for the stationary nucleation rate around a growing stable cluster.^{2,30}

The expression for the local distribution of the stationary nucleation rate, $J_{st}(\rho)$, around a growing cluster of radius r is predicted by atomistic theory³⁰

$$J_{st}(\rho) = K_1 [c(\rho)]^{1-\alpha} \exp\left[\frac{(n_k + \alpha)nF\eta(\rho)}{RT}\right] \quad (14)$$

where $K_1 = \gamma Z_0 \exp[-\phi(n_k)/(kT)]$, γ is a frequency factor, Z_0 is the number of sites available for nucleation, and $\phi(n_k)$ is the interfacial energy required for the creation of a critical nucleus of n_k atoms. ρ is measured from the edge of the particle.

For a system under combined diffusion and charge-transfer control, the ratio of the nucleation rate at a distance ρ from a growing cluster to that on the cluster-free surface is given by²

$$\frac{J_{st}(\rho)}{J_{st}^0} = \left[1 - \frac{r}{\rho} \left(1 - \frac{c_s}{c_\infty}\right)\right]^{(1+n_k)} \quad (15)$$

where the ratio c_s/c_∞ can be determined from eq 10. By calculating the growth of a particle with time using eq 11, we can determine the distribution of relative nucleation rates surrounding that growing particle with time. An example of this is provided in semilogarithmic form in Figure 7a, in which the distribution of $J_{st}(\rho)/J_{st}^0$ as a function of distance from the growing particle is plotted as a function of time after the nucleation of that particle. We have chosen the parameters to be the same as those used within our experiments and an overpotential that was sufficiently high that the particle growth is under diffusion control. It can be seen that the relative nucleation rate has a sigmoidal form in the semilogarithmic plot and that with time the distribution shifts to greater distance scales.

If we consider that when $J_{st}(\rho)/J_{st}^0$ falls to a low enough value the likelihood of nucleating another particle is sufficiently low that it can be ignored, then we can get an estimate of the exclusion area around the growing particle under different conditions. We relabel the parameter $J_{st}(\rho)/J_{st}^0$ as the nucleation cutoff parameter, J_{rel} , and solve eq 15 for ρ while substituting in eq 10

$$\rho = \frac{r^3}{2Dc_\infty V_M t (1 - J_{rel}^{1/(1+n_k)})} \quad (16)$$

Substituting in eq 11 for the radius as a function of time, we obtain the cumbersome expression for ρ as a function of time during the growth of a particle under combined diffusion and charge-transfer control

$$\rho(t) = \frac{(\sqrt{A^2 + 8ABV_M t} - A)^3}{16Dc_\infty V_M C^3 t (1 - J_{rel}^{1/(1+n_k)})} \quad (17)$$

where A , B , and C have been previously defined. This equation provides the distance from the edge of the growing particle

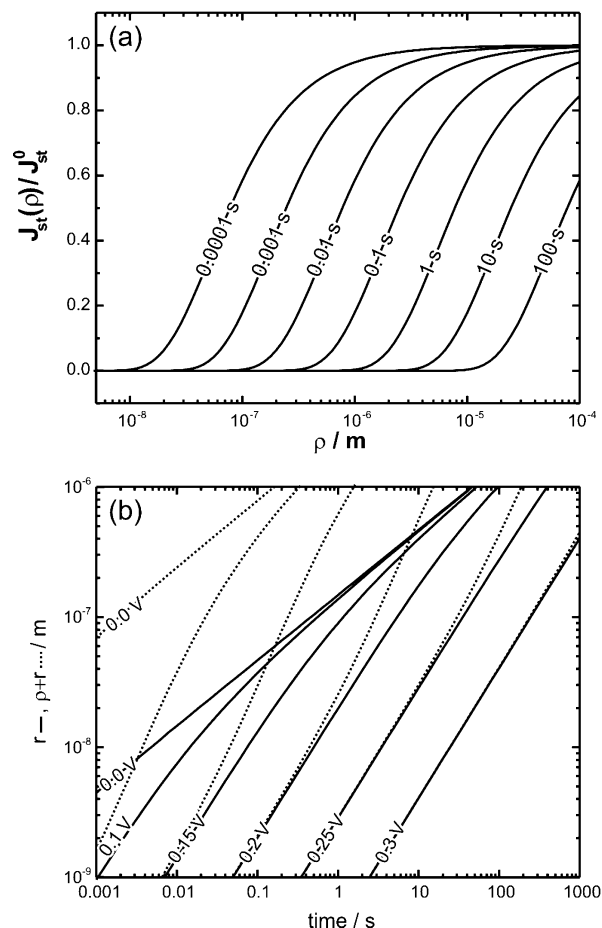


Figure 7. (a) Distribution of relative local nucleation rate at a distance ρ from a growing Pt particle at different times after the particle is nucleated; (b) calculated radius (r , —) and nucleation exclusion radius ($\rho + r$, ···) for the nucleation of a Pt particle as a function of applied potential. The solution is assumed to contain $0.001 \text{ mol dm}^{-3} \text{ H}_2\text{PtCl}_6$. The parameters used for the simulation were $j_0 = 8 \times 10^{-6} \text{ A cm}^{-2}$, $D = 1.2 \times 10^{-5} \text{ cm}^2 \text{ s}^{-1}$, $T = 298 \text{ K}$, $\alpha n = 1$, $J_{rel} = 0.1$. The potentials displayed are comparable to the experimentally applied potentials (i.e., the overpotentials used in the equation have been converted to the SCE scale).

within which the nucleation rate has fallen to below J_{rel} of that on the free surface.

In Figure 7b, we plot as a function of time the calculated radius of a growing particle as a function of the applied potential (ΔE , solid lines). The parameters used are the same as those used in (and determined from) our experiments. We see that as the overpotential is increased (i.e., the applied potential decreased) there is a transition from electrocrystallization control to diffusion control. If the applied potential is 0 V or below, the growth is entirely dictated by mass transport of reactants to the surface, and the response becomes independent of applied potential. Also plotted in this diagram is the distance from the center of the particle over which the nucleation rate is reduced to one tenth of the nucleation rate on the unmodified surface, determined from eq 17 (i.e., $J_{rel} = 0.1$, dotted line). At low overpotentials (i.e., applied potentials of 0.3 V), the nucleation exclusion zone extends only very slightly beyond the edge of the particle over the entire time span. As the overpotential is increased, the rate at which ρ increases starts outstripping the growth of the particle. At 0.25 V, ρ is as large again as r after about 90 s of polarization; at 0.2 V, this occurs at 2 s after the start of growth of the particle. At still higher overpotentials (i.e., lower applied potentials), the time at which ρ is twice as large

as r shifts to shorter and shorter values. Indeed, at an applied potential of 0.0 V, ρ is 15 times larger than the radius of the particle a mere 0.001 s after particle growth begins.

Figure 7b allows us to rationalize the results presented above and to understand why we do not see multiple nucleation at “large” electrodes (~ 100 nm, bearing in mind that our “large” electrodes are still much, much smaller than the typical microelectrodes used in studies of particle nucleation and growth) under conditions of high overpotential yet appear to have multiple nucleation on the same electrode when we are under electrocrystallization control.

At low overpotentials, there is virtually no reduction in the nucleation rate on the electrode adjacent to the growing nucleus. Thus, to be assured of seeing only a single nucleation–growth transient, it is necessary to limit the size of the underlying electrode. In our case, we find that the electrode cannot have a radius of more than about 5 nm, Figure 4a,b, and Figure 5a, curves iii and iv. Furthermore, under these conditions, the growing particle obscures the underlying electrode within a few seconds after the start of its growth. In comparison, on electrodes larger than about 5 nm, not only is there no reduction in the nucleation rate of the unobscured electrode, but the growth of any particle is slow enough so that it can take a significant time to obscure the electrode. Hence on larger electrode, there is a significant chance of multiple nucleation and growth, Figure 5a, curves i and ii.

Under conditions of high overpotential, Figure 6, we obviously still expect single nucleation and growth on very small electrodes (~ 1 nm), especially because the nucleation exclusion zone will be much larger than the underlying electrode even at short time. The situation is similar for large (~ 100 nm) electrodes. At deposition potentials of 0.0 V and below, the size of the nucleation exclusion zone is as large as the electrode within about 1 ms of particle growth commencing. Thus, to have a reasonable chance of nucleating further particles at other points on the electrode, it would be necessary for them to form within those crucial few milliseconds. They are unlikely to form after that elapsed time, and if they formed beforehand, then their growth would have, in all likelihood, prevented the nucleation of the particle that we are considering. If the nucleation rate on the electrode surface were high, then there still might be the chance of nucleating further particles on the electrode (our nucleation exclusion zone represents the area where the nucleation rate has dropped by 1 order of magnitude), but if this were the case, then we would not have a significant delay after polarization before we saw the rising current transient. Thus it is reasonable to assume that even on “large” electrodes, we see the nucleation of only one particle. In the unlikely event that more than one particle were formed, those particles would merge within a few seconds on a 100 nm electrode.

We have assumed that the substrate is planar, but in reality our carbon nanoelectrodes may show some deviation from this geometry, for instance, elongated cones or hemispheroids. The variation of substrate geometry would also affect the geometry of the growing nuclei. We have assumed that the growing particles possess a semispherical geometry, although in reality the particles may be ovoid or irregularly shaped. Finally, it is assumed that the current efficiency for the production of platinum metal is 100% during the entire deposition process. We have measured the size of the Pt particles produced during these experiments using SEM microscopy and compared the volume of material in the particle to that expected if the current efficiency were 100%. In these calculations, we must make a number of assumptions, namely, that the particle is fully compact

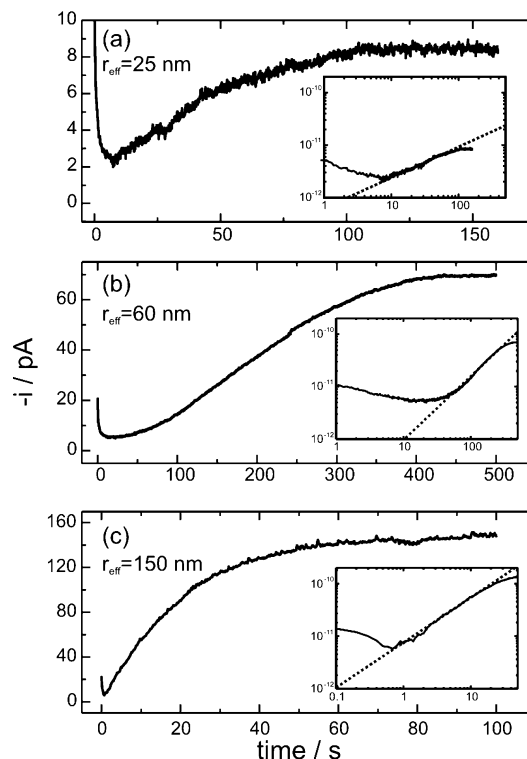


Figure 8. Current–time curves upon potential steps to (a) 0.3, (b) 0.3, and (c) 0.28 V obtained at carbon electrodes of (a) 25, (b) 60, and (c) 150 nm in $0.1 \text{ mol dm}^{-3} \text{ H}_2\text{SO}_4 + 0.001 \text{ mol dm}^{-3} \text{ H}_2\text{PtCl}_6$. Inset are the corresponding $\log(i)$ – $\log(t)$ curves.

(i.e., it has a density that is the same as bulk platinum), and we must assume something about the volume of the material in the particle (e.g., in Figure 2, it is necessary to assume that the cone of the underlying carbon electrode penetrates to the center of the spherical particle), and so there is a relatively large error associated with calculating these current efficiencies. Nonetheless, in all cases, we find efficiencies in excess of 50%, and we believe that the actual value is around 70–90%. Thus, under diffusion-controlled conditions, the majority of the reduction continues all the way to platinum metal, and relatively little PtCl_4^{2-} escapes into solution.

3.3. Current Transients Accompanying Platinum Deposition with a Nucleation and Growth Mechanism—Multiple Nuclei. In the previous section, we have demarcated the conditions under which single-particle nucleation and growth is expected to predominate. But what happens when the conditions of the experiment are outside of these regimes?

Displayed in Figure 8 are diagrams for the transients obtained at electrodes of radius 25, 60, and 150 nm at an applied potential of 0.3 V (0.28 V for the largest electrode). Under these conditions, the growth of any particle will predominantly be under electrocrystallization control. Because of the relatively slow rate of particle growth and thus the low rate of consumption of reactants, the nucleation exclusion zone extends only a very small distance from any growing nucleus. Furthermore, because the growth of the particles is slow, they will take some time to obscure the underlying electrode. Indeed, on the smallest electrode, Figure 7b suggests that it would take over 100 s for the growing particle to cover the electrode surface, allowing ample opportunity for further nuclei to form. On the larger electrodes, this time delay would be even greater and the formation of extra nuclei correspondingly more likely.

If nucleation of multiple nuclei occurs, the interference between the individual growing particles renders the theoretical

analysis of the overlap problem much more complicated. The current transients can be modeled by introducing Avrami's approximation^{12,31,32} to deal with the overlap problem and two extreme cases for the nucleation rate are assumed, that is, the instantaneous nucleation case in which all the nuclei are immediately created at the beginning of the experiment with their numbers remaining constant during the growth process and the progressive nucleation case in which new nuclei are continuously formed during the whole deposition process.

The main difference between the multiple nucleation and single nucleation case is that in the former process the current increase due to enlargement of the nuclei will slow after a period of time because of overlap of the diffusion hemispheres of the growing nuclei, and after this point in time, there will be a current maximum or plateau. For instantaneous nucleation of multiple nuclei, the current transient during the initial rising section where overlap does not occur should have a similar form to eqs 5 and 6 but multiplied by a factor representing the total number of nucleation sites on the surface, N_0 .

Under conditions for which nucleation is not instantaneous, the situation is more complex. Scharifer and Hill³³ have provided detailed experimental results that show that the rate of growth is significantly less than that predicted by the previous case for instantaneous nucleation.^{34,35} Indeed, several different approaches have been used to model the potentiostatic current transient occurring during progressive three-dimensional nucleation with growth under diffusion control. In all cases, they are based on comparable models but tend to produce significantly different results. Three broad approaches may be demarcated: that of Mirkin and Nilov³⁶ (also independently derived by Heerman et al.³⁷), that of Sluyters-Rehbach et al.³⁸ and that of Sharifker and Mostany.³⁹ Sharifker et al. have compared all three approaches in fitting real experimental data and in fitting transients produced from computer simulations (for which the underlying values of N_0 and A , the nucleation rate per active site, are known).⁴⁰ At sufficiently short times ($At \rightarrow 0$), for which there is no significant overlap of the diffusion spheres, they find that all three results converge to an $(At)^{3/2}$ dependency. For progressive nucleation, a time-dependent nuclei number has to be incorporated into the current expression and linearity of $I-t^3$ or $I-t^{3/2}$ holds for electrocrystallization-controlled or diffusion-controlled deposition, respectively. In our cases, the time exponent of the rising part of the transient is calculated by fitting the linear section of the $\log(i)-\log(t)$ plots, Figure 8 (inset). We find a wide range of time exponents, 0.585 ± 0.005 for the 25 nm electrode, 1.216 ± 0.002 for the 60 nm electrode, and 0.857 ± 0.005 for the 150 nm electrode. Thus these transients do not clearly fit any of the established theories for multiple nucleation-growth. These theories are statistically based, and our results may be skewed because they undoubtedly involve the nucleation of a relatively small number of sites and may thus not represent a statistically averaged response. Thus it would appear difficult at this stage to study multiple nucleation and growth on very small electrodes because of the small number of events that are liable to occur.

Another unique feature of the nucleation and growth process at nanometer-sized substrates is that the overlap process occurs at very short time and a single growth center is relatively quickly established. At macroscopic electrodes, the limiting current plateau in the current transient during electrocrystallization-controlled 3-D growth of multiple nuclei would last a considerable time because of the deposition area being kept relatively constant when the overlap process finishes.^{31,32} The increase in electrode area due to deposition is negligible because the total

substrate area is very large. However, in our case, the extremely small electroactive areas ensure the nucleation of only a very small number of nuclei. Once the overlap finishes, a new single growing center will be formed. Continuous deposition will increase the total interfacial area as the particle grows resulting in further increases of current. Such transients have indeed been observed.

4. Conclusion

In this paper, we have shown that nanometer-sized electrodes are a useful tool in studying the initial deposition steps even in the presence of another electroactive process. Studies of electrodeposition on these electrodes can yield useful insights into the nucleation and growth mechanism. The extremely small electroactive area of the substrate opens up the possibilities of observing single nucleation and growth processes, in which kinetic and mechanistic analysis will be greatly simplified. We demarcate two distinct regimes in which single nucleation can be discerned. Under electrocrystallization control, that is, at low overpotentials, we are likely to observe single nucleation and growth when we use electrodes with radii less than about 5 nm. On these electrodes, the rate of growth of the particle is such that it covers the underlying electrode within a second or so. The other regime in which single nucleation can be forced is under conditions of high overpotentials for which the reaction is predominantly under diffusion control. Under these conditions, there is the rapid formation of a nucleation exclusion zone, which effectively stops the formation of secondary nuclei on the electrode. For our system, we can increase the underlying electrode size to about a few hundred nanometers and still see single nucleation and growth.

We find that the diffusion coefficient of the PtCl_6^{2-} anion is $(1.2 \pm 0.1) \times 10^{-5} \text{ cm}^2 \text{ s}^{-1}$ and the exchange current density for the reduction reaction of that species to metallic Pt is $(8 \pm 1) \times 10^{-6} \text{ A cm}^{-2}$.

Acknowledgment. We gratefully acknowledge financial support by the Leverhulme trust under Grant F/07 058/C. We also thank Mr. Peter Hope from LVH for kindly providing the electrophoretic paint solution. Mr Simon Turner in the Chemistry Department of Imperial College London is thanked for his workshop skills.

References and Notes

- (1) Fletcher, S. J. *Cryst. Growth* **1983**, *62*, 505.
- (2) Kruijt, W. S.; Sluytersrehbach, M.; Sluyters, J. H.; Milchev, A. J. *Electroanal. Chem.* **1994**, *371*, 13.
- (3) Antonie, O.; Durand, R. *Electrochem. Solid-State Lett.* **2001**, *4*, A55.
- (4) Gloaguen, F.; Leger, J. M.; Lamy, C.; Marmann, A.; Stimming, U.; Vogel, R. *Electrochim. Acta* **1999**, *44*, 1805.
- (5) Zoval, J. V.; Lee, J.; Gorer, S.; Penner, R. M. *J. Phys. Chem. B* **1998**, *102*, 1166.
- (6) Liu, H.; Penner, R. M. *J. Phys. Chem. B* **2000**, *104*, 9131.
- (7) Watanabe, M.; Sei, H.; Stonehart, P. *J. Electroanal. Chem.* **1989**, *261*, 375.
- (8) Gamez, A.; Richard, D.; Gallezot, P.; Gloaguen, F.; Faure, R.; Durand, R. *Electrochim. Acta* **1995**, *41*, 307.
- (9) Friedrich, K. A.; Henglein, F.; Stimming, U.; Unkauf, W. *Electrochim. Acta* **2000**, *45*, 3283.
- (10) Bregol, L. J. *Electrochim. Acta* **1978**, *23*, 489.
- (11) Gunawardena, G.; Hills, G.; Scharifker, B. R. *J. Electroanal. Chem.* **1981**, *130*, 99.
- (12) Heerman, L.; Tarall, A. *J. Electroanal. Chem.* **1998**, *451*, 101.
- (13) Li, L. J.; Fleishmann, M.; Peter, L. M. *Electrochim. Acta* **1989**, *34*, 459.

- (14) Fleishmann, M.; Pons, S.; Daschbach, J. In *Microelectrode: Theory and Application*; Montenegro, M. I., Queirós, M. A., Daschbach, J. L., Eds.; Kluwer: Netherlands, 1991.
- (15) Hills, G.; Pour, A. K.; Scharifker, B. *Electrochim. Acta* **1983**, *28*, 891.
- (16) Chen, S. L.; Kucernak, A. *Electrochem. Commun.* **2002**, *4*, 80.
- (17) Chen, S. L.; Kucernak, A. *J. Phys. Chem. B* **2002**, *106*, 9396.
- (18) Georgolios, N.; Jannakoudakis, D.; Karabinas, P. *J. Electroanal. Chem.* **1989**, *264*, 235.
- (19) Zubimendi, J. L.; Vazquez, L.; Ocon, P.; Vara, J. M.; Triaca, W. E.; Salvarezza, R. C.; Arvia, A. J. *J. Phys. Chem.* **1993**, *97*, 5095.
- (20) Shimazu, K.; Weisshaar, D.; Kuwana, T. *J. Electroanal. Chem.* **1987**, *223*, 223.
- (21) Jiang, J.; Kucernak, A. *J. Phys. Chem. B*, submitted for publication.
- (22) Hills, G. J.; Schiffrin, D. J.; Thompson, J. *Electrochim. Acta* **1974**, *19*, 657.
- (23) Bard, A. J.; Parsons, R.; Jordan, J. *Standard Potentials in Aqueous Solutions*; Marcel Dekker: New York, 1985.
- (24) Cai, J. L.; Pletcher, D. *J. Electroanal. Chem.* **1983**, *149*, 237.
- (25) Kelaidopoulou, A.; Kokkinidis, G.; Milchev, A. *J. Electroanal. Chem.* **1998**, *444*, 195.
- (26) Sluyters, J. H.; Bosco, E.; Sluytersrehabach, M. *J. Electroanal. Chem.* **1988**, *241*, 79.
- (27) Sluyters, J. H.; Wijenberg, J.; Mulder, W. H.; Sluytersrehabach, M.; Bedeaux, D. *J. Electroanal. Chem.* **1989**, *261*, 263.
- (28) Markov, I.; Boynov, A.; Toshev, S. *Electrochim. Acta* **1973**, *18*, 377.
- (29) Milchev, A.; Vassileva, E.; Kertov, V. *J. Electroanal. Chem.* **1980**, *107*, 323.
- (30) Milchev, A.; Kruijt, W. S.; Sluytersrehabach, M.; Sluyters, J. H. *J. Electroanal. Chem.* **1993**, *362*, 21.
- (31) Armstrong, R. D.; Fleischmann, M.; Thirsk, H. R. *J. Electroanal. Chem.* **1966**, *11*, 208.
- (32) Thirsk, H. R.; Harrison, J. A. *A Guide to the Study of Electrode Kinetics*; Academic Press: London and New York, 1972.
- (33) Scharifker, B.; Hills, G. *Electrochim. Acta* **1983**, *28*, 879.
- (34) Toshev, S.; Milchev, A.; Vassileva, E. *Electrochim. Acta* **1976**, *21*, 1055.
- (35) Milchev, A.; Scharifker, B. R.; Hills, G. J. *J. Electroanal. Chem.* **1982**, *132*, 277.
- (36) Mirkin, M. V.; Nilov, A. P. *J. Electroanal. Chem.* **1990**, *283*, 35.
- (37) Heerman, L.; Matthijs, E.; Langerock, S. *Electrochim. Acta* **2001**, *47*, 905.
- (38) Sluyters-Rehbach, M.; Wijenberg, J.; Bosco, E.; Sluyters, J. H. *J. Electroanal. Chem.* **1987**, *236*, 1.
- (39) Scharifker, B. R.; Mostany, J. *J. Electroanal. Chem.* **1984**, *177*, 13.
- (40) Scharifker, B. R.; Mostany, J.; Palomar-Pardave, M.; Gonzalez, I. *J. Electrochem. Soc.* **1999**, *146*, 1005.